Mean-field study of the role of lateral cracks in microtubule dynamics

Gennady Margolin, Holly V. Goodson, and Mark S. Alber

Phys. Rev. E **83**, 041905 — Published 8 April 2011

DOI: 10.1103/PhysRevE.83.041905

Mean-field study of the role of lateral cracks in microtubule dynamics

Gennady Margolin,[1,2] Holly V. Goodson,[3,2] and Mark S. Alber[1,2,*]

[1]*Department of Applied and Computational Mathematics and Statistics*
[2]*Interdisciplinary Center for the Study of Biocomplexity*
[3]*Department of Chemistry and Biochemistry*
University of Notre Dame, Notre Dame, IN 46556, USA

A link between dimer-scale processes and microtubule (MT) dynamics at macro-scale is studied by comparing simulations obtained using computational dimer-scale model with its mean field approximation. The novelty of the mean field model (MFM) is in its explicit representation of inter-protofilament cracks, as well as in the direct incorporation of the dimer-level kinetics. Due to inclusion of both longitudinal and lateral dimer interactions, the MFM is two-dimensional, in contrast to previous theoretical models of MTs. It is the first analytical model that predicts and quantifies crucial features of MT dynamics such as (i) existence of a minimal soluble tubulin concentration needed for the polymerization (with tubulin values represented as a function of model parameters), (ii) existence of steady-state growth and shortening phases (given with their respective velocities), and (iii) existence of an unstable pause state near zero velocity. In addition, the size of the GTP cap of a growing MT is estimated. Theoretical predictions are shown to be in good agreement with the numerical simulations.

PACS numbers: 87.16.Ka, 82.35.-x, 05.40.-a

I. INTRODUCTION

Microtubules (MTs) are polymers that are found in all eukaryotes. They play crucial role in cell division, participate in cell movements by regulating cell polarity, and serve as tracks for molecular motors. MTs in cells typically display rapid fluctuations in length in order to explore cellular space and find targets of attachment. This behavior is known as dynamic instability [1, 2], and it is characterized by frequent transitions from growth to shortening, termed catastrophes, and from shortening to growth, termed rescues. The observation that MTs assembled from purified tubulin display dynamic instability indicates that this behavior is intrinsic to MTs.

Structurally, MTs are hollow cylinders, or tubes, typically formed by 13 protofilaments aligned along the tube axis. Each protofilament is a linear chain of alpha-beta tubulin heterodimers, all facing in the same direction and conferring polarity to the MT: the plus end has the beta monomers exposed. The subunits in the protofilaments are arranged in a B lattice except at the seam, where there is a helical shift of three monomers between the first and last protofilaments, resulting in an A lattice. In a B lattice, alpha monomers laterally bind alpha monomers and beta bind beta, while in an A lattice, alpha monomers bind laterally to beta. Structural studies suggest that the longitudinal bonds between the heterodimers are significantly stronger than the lateral contacts [3, 4].

MTs evolve by exchange of heterodimers between solution and the MT ends. Typically, the plus end is exposed and evolves, while the minus end is nondynamic because it is attached to a nucleation site. The heterodimers in solution bind the nucleotide GTP, which hydrolyzes to GDP after polymerization, incurring conformational changes. Importantly, there is a delay in hydrolysis, leading to a formation of a GTP cap, which has a stabilizing effect on the growing MT tube. The rest of the MT, however, consists of GDP-bound tubulin that depolymerizes as soon as the cap is lost [5, 6]. (Note that GDP cannot be exchanged for GTP until a subunit depolymerizes). Dynamic instability is thus thought to be the consequence of frequent formation and loss of the GTP cap.

After Hill and Chen [7] proposed an effective two-state model of MT dynamic instability in 1984, mainly two approaches have been used to study MTs. One approach postulates macroscopic rates of dynamic instability (see [7]). The second approach is to construct a dimer-scale numerical model of a single MT (see [8]). There are also some theoretical and numerical approaches [8–14] that consider linear, "one-protofilament" MTs and model the stabilizing cap. Finally, there are models of MTs that explicitly incorporate energetics [15–18]. However, except for [17], whose modeling of MT dynamics is also numerical, these models do not address MT growth and/or shortening but instead focus on stability of the MT tube.

In this paper, a direct link is established between the dimer-scale processes and the MT dynamics at macro-scale. Namely, our theoretical mean field model (MFM) directly incorporates parameters from the Monte-Carlo dimer-scale model to yield a macroscopic description.

*Electronic address: malber@nd.edu

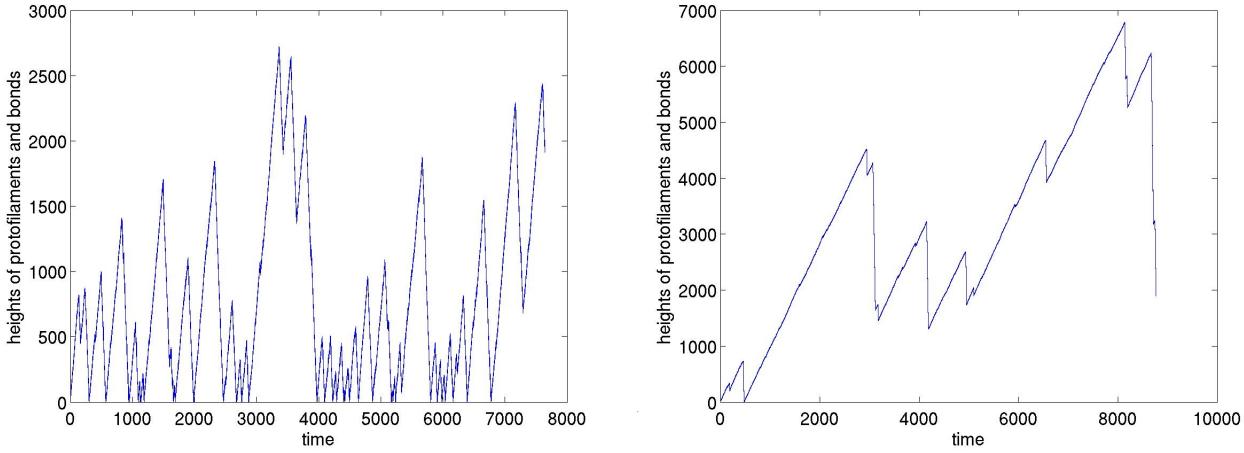

Figure 1: (Color online) Examples of length history plots for parameter sets 3m (left) and S8 (right) with [Tu]= $14\mu M$ and $10\mu M$, respectively. Each simulation is 10^7 steps long. Note that the scales are different. See Section II B for details.

The most important distinguishing feature of our approach, in comparison with previous dimer-scale models [4, 19–22], is its explicit treatment of lateral bonds. Specifically, chains of bonds between two neighboring protofilaments grow and shorten (due to the formation and breakage of bonds between individual subunits) just as the protofilaments themselves can grow and shorten. This allows for the formation of frayed ends and curled protofilaments observed experimentally (the so called "ram's horns" [23, 24]). This feature is important because these curled, laterally unbonded protofilaments have significant influence on microscopic processes at MT tips, particularly rescue.

VanBuren et al. [4] developed a stochastic kinetic model elucidating MT assembly dynamics. They recognized the importance of modeling ram's horns and to address this question among others, later developed a mechanochemical model [17, 25] based on elastic energy considerations between neighboring dimers. In our model, the impact of mechanical influences, such as the energetic barriers to forming lateral bonds between curling protofilaments, is incorporated into the kinetic rate constants governing the different dimer-scale events, in the spirit of [4]. The main advantage of using the kinetic approach, instead of the mechanochemical one, is that it is orders of magnitude faster. This allows one to simulate experimentally relevant time spans (tens of minutes), which results in observing in simulations both catastrophes and rescues and generating experiment-like "life history" plots which are needed for analysis of dynamic instability parameters (see Figure 1).

Kolomeisky and colleagues [26, 27] have developed a growth model of rigid multiprotofilament biopolymers, such as actin and MTs. Their theoretical approach reduces the problem to a "one-layer" model [26], in which only two possible events can happen in any given configuration of MT tip: polymerization on the shortest or depolymerization on the longest protofilament. (Numerical simulations [27] do not have this restriction.) This simplification yields analytic expressions for MT growth velocity and dispersion. However, the authors study only the polymer growth, and their model allows neither interprotofilament cracks, nor GTP hydrolysis. Brun et al. [28] focused on studying the occurrence and characteristics of a catastrophe. Hence, their work does not consider dynamic instability, and it also does not allow cracks. In this paper, we study both growth and shortening, model cracks and allow hydrolysis.

In Section II, a dimer-scale numerical stochastic model of an MT and numerical study of dynamic instability are described. Then, in Section III, a mean-field theoretical approach is introduced and applied to the problem. Finally, results obtained using these two approaches are compared with each other.

II. DESCRIPTION OF COMPUTATIONAL MONTE CARLO MODEL AND SIMULATIONS

A. Overview of the model

We treat the MT as a lattice domain bent on itself forming a tube with a seam. Tube walls are the protofilaments, extending along the tube axis, and the seam is due to the 1.5 dimers shift between the first and the last protofilaments. Normally the MT has 13 protofilaments, but this can vary. The MT subunits (tubulin heterodimers) have two states, one prone to polymerization and the other prone to disassembly. These states are denoted as GTP-Tu and GDP-Tu, but they could represent other conformational states. Finally, the model dynamics is based on five events: protofilament growth, protofilament shortening, inter-protofilament bond growth (bonding), inter-protofilament bond shortening (breakage), and the transition of GTP-Tu to GDP-Tu, i.e. GTPase

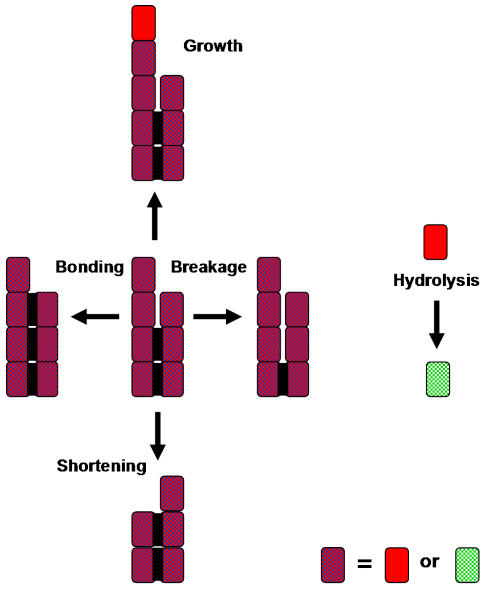

Figure 2: (Color online) Schematic representation of processes (possible events) in the microtubule model. Red homogeneous and bright checkered rectangles are GTP-Tu and GDP-Tu dimers, respectively. Dark checkered rectangle is any dimer.

activity (hydrolysis) - cf. Figure 2. We assume that subunits add as individual dimers, but laterally unbonded sections of protofilament can break at any position, leaving open the possibility that multiple subunits detach simultaneously. The GTPase is modeled as a simple first-order event that occurs only on internal subunits, consistent with structural evidence that alpha monomers act as GAPs (GTPase activating proteins) for beta monomers [29]. These events occur at the level of individual dimers and are governed by kinetic rate constants that are set by the user. (Additional details are given in Appendix A.) Simulations presented in this paper use two different sets of reference parameters, denoted as "3m" and "S8", chosen to be consistent with the existing range of estimates of inter-dimer bond energies and to give rise to transition frequencies that are in agreement with those observed in experiments. (See their description and comparison to other papers in Appendix B.)

B. Recapitulation of dynamic instability

We performed Monte Carlo simulations with two parameter sets described in Appendix B. For each set, we used different concentrations of free GTP-Tu [Tu] and then calculated dynamic instability (DI) parameters: growth velocity (v_g), shortening velocity (v_s), catastrophe frequency (f_c) and rescue frequency (f_r), based on the generated length history plots. Typical length history plots are shown in Figure 1. The final results are plotted in Figures 3 and 4. The velocities are given in dimer lengths/aut (arbitrary units of time) and the frequencies in inverse aut. If one aut is set to 1 second and the dimer length is set at the experimentally measured value of 8nm, these values are consistent with the range of values obtained in *in vitro* observations [30–32]. We used a thresholding algorithm to define the phase transitions (catastrophes and rescues), based on a length history of the average protofilament length. A phase transition was accepted if the average length changed by more than h dimers in the direction opposite the current phase (e.g., if during current growth phase there was a drop in average length by more than h dimers compared to any preceeding average length within the current growth phase). As a technical note, our algorithm underestimates v_s and f_r when the length fluctuations are small. The error in the ratio v_s/f_r is much smaller, and we used this ratio to correct the value of f_r by keeping v_s constant. Inspection of length history plots (not shown) shows that, indeed, v_s is independent of [Tu]. See more details in Appendix D.

Additionally, we monitored the number of GTP-Tu dimers in the MT during growth, the laterally bonded GTP cap length, and the crack depths (i.e.,the lengths of laterally unbonded regions between protofilaments) during growth and shortening. These results are summarized in Table I for [Tu]$=14$ and $10\mu M$ for sets 3m and S8, respectively. There are two ways to estimate the crack depth in the simulations. First, we can simply measure the average crack depth (d) between all pairs of adjacent protofilaments. For each pair, d would equal the length of the unbonded part of the shortest of the two protofilaments. Second, we can calculate Δ, which is defined as the mean protofilament length minus mean bond length. When all protofilaments are of the same length, these two estimates coincide.

Finally, we measured the single-step decreases/drops in MT length during growth phase. The MT length was defined as the length of the longest protofilament. We find that MT shortens by 3.2 ± 2.5 and 1.4 ± 0.7 dimers per MT length drop for

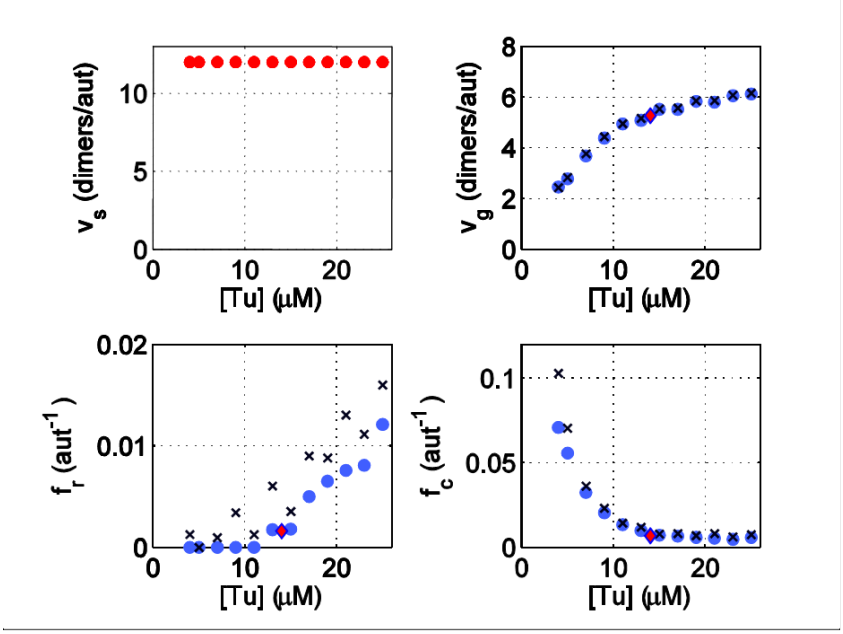

Figure 3: (Color online) Dependence of DI parameters of set 3m on [Tu]. Black x's and blue circles are for the phase transition thresholds of 10 and 20 dimers in length, respectively. (When [Tu] is low and MTs are short, higher thresholds fail to resolve individual short growth phases, significantly underestimating all the DI parameters. See Appendix D.) They are based on single runs of 10^7 steps. Red diamonds are averages of five runs with a threshold of 100 dimers. aut - arbitrary units of time.

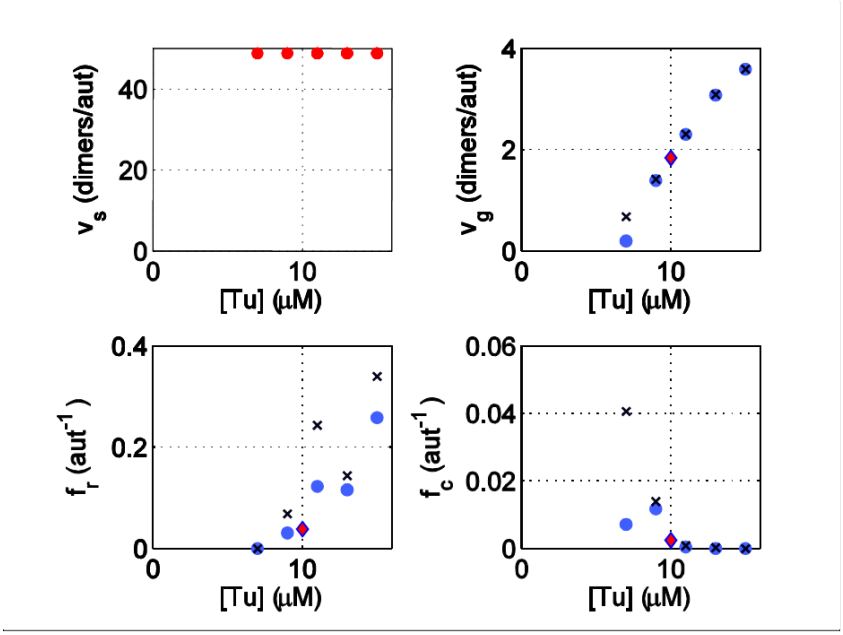

Figure 4: (Color online) Dependence of DI parameters of set S8 on [Tu]. Symbols are as in Figure 3. Red diamonds are averages of five runs with a threshold of 50 dimers. The apparent simultaneous reduction in v_g and f_c at 7μM for threshold 20 (blue circles) is an artifact of our procedure to extract DI parameters, due to short MTs at this concentration. aut - arbitrary units of time.

	N_T	ℓ_b	d_g	Δ_g	d_s	Δ_s
3m	450	25	5	8	7	10
S8	130	7	1	1.6	1.5	2.5

Table I: Simulation estimates of the number of GTP-Tu during growth (N_T), laterally bonded GTP cap during growth (ℓ_b), and crack depths (d and Δ), during growth and shortening. The values are for the sets 3m and S8 with [Tu]= 14 and 10μM, respectively.

sets 3m and S8 at 14 and 10μM, respectively. This indicates that for chosen parameters, oligomers can detach from unbonded protofilament tips. This conclusion contradicts [25], which argues that both polymerization and depolymerization during growth phase occur overwhelmingly by single dimer addition and loss. We suggest that one explanation for this difference is that in [25], the growing tip of an MT was held at the solid wall, which would hinder incorporation of dimers especially to the longest protofilament. This would be expected to reduce the length of protofilament extensions, and in turn reduce the likelihood of observable oligomer detachment.

How much undestanding of these simulations can be achieved from purely theoretical analysis? In what follows, we develop a mean-field theoretical model (MFM) and compare its predictions with the results obtained using MTs described above.

III. THEORETICAL APPROXIMATIONS

After describing Monte Carlo simulations, we turn to a theoretical approach. The aim is to develop a better intuitive understanding of the numerical model and, it is believed, of real microtubules. Ideally, given the set of dimer-scale parameters, we would like to predict the growth and shortening velocities, as well as transition frequencies. We would also like to predict some characterisitics of a GTP-Tu cap, e.g. its size. As seen below, we make substantive progress with the theory, even though the phase transitions remain to be studied. In our theoretical approximations, we make a few assumptions. Initially, in Section III A, we consider a microtubule (MT) consisting of only one type of heterodimer, e.g., either all GTP-Tu, all GDP-Tu or all GMPCPP-Tu. This approximation will be relevant to real MTs, either in the case of relatively long GTP-cap or in the case of MT shortening, when the tip configuration is defined, wholly or predominantly, by dimers of the same type. In Section III B, this restriction is lifted, and we consider hydrolysis. Also, we make a "mean-field" approximation, and in particular, do not consider the MT seam specifically.

A. One-dimer-type MT approximations

Since currently there are no dimer interconversions, the MT dynamics can be described as a Markovian process using only the lengths of protofilaments and of their lateral contacts (bonds). Our goal is to obtain estimates of MT dynamics and tip structure. Specifically, we make predictions of MT growth and/or shortening velocities, v_∞ (eq.(7)) and of the interprotofilament crack depth d_∞ (eq.(6)). These values are in reasonable agreement with numerical simulations (the theoretical and simulated values can differ by a factor of 2 or 3 for considered parameter sets) and hence can serve as an initial guide for the parameter choice.

Let $p_i(t)$ and $b_i(t)$ be the lengths of the ith protofilament and of the interprotofilament lateral formed ("zipped") bond between the ith and (i+1)'th protofilaments, respectively, at time t (in units of a dimer length). Then, with a lateral bonding rate of K_{bond} (Section II and Appendices A, B) and introducing an effective lateral breakage rate $K_{break,eff}$ (see below),

$$\dot{b}_i(t) = -K_{break,eff} H(b_i(t) \geq 1) + K_{bond} H(p_i(t) \geq b_i(t)+1) H(p_{i+1}(t) \geq b_i(t)+1), \tag{1}$$

where the dot over the variable denotes temporal derivative, and the Heaviside function H is defined as 1, if the condition in brackets is true, and 0 otherwise. These conditions are necessary for the breakage or bonding to be possible. The first condition is a boundary condition, while the second and the third conditions state that to form a lateral bond there should be pre-existing neighboring protofilaments between which this bond can form. If there are n protofilaments, then, disregarding the seam shift, we can introduce the periodic boundary condition by setting $p_{n+1}(t) \equiv p_1(t)$. The ith protofilament can shorten by no more than $p_i - \max(b_{i-1}, b_i)$, which is the length of its laterally unbonded end, and of course $b_0(t) \equiv b_n(t)$. Therefore, considering all possible shortening events by s dimers,

$$\dot{p}_i(t) = K_{grow} - \sum_{s=1}^{p_i(t)-\max(b_{i-1}(t),b_i(t))} s K_{shorten}, \tag{2}$$

where K_{grow} is the polymerization rate and $K_{shorten}$ is the rate of breakage of a longitudinal (intra-protofilament) bond. (See Appendices A, B.) The values of K_{break}, K_{bond}, K_{grow} and $K_{shorten}$ are given, and K_{grow} depends on the concentration of soluble tubulin, [Tu]. In our computational model, the lateral breakage rate of ith bond is K_{break} unless both $b_{i-1}(t) \geq b_i(t)$ and $b_{i+1}(t) \geq b_i(t)$. In that case, the lateral breakage rate is reduced to K_{break}/π_{break} to reflect the steric constraints, due to a partially or fully closed cylindrical MT body. When the lateral bond breaks the participating dimers have to move at least slightly away from each other. This movement is hindered by the presence of the surrounding dimers, especially when there is a fully formed MT tube near the considered locus. The simplest way to take this into consideration here is to calculate the probability q that for a randomly picked bond its two neighboring bonds are not shorter than it is. Then we will approximate $K_{break,eff} = (1-q)K_{break} + qK_{break}/\pi_{break}$. It is easy to argue that the probability of having N independent, identically distributed (iid) random numbers to be greater or equal to another randomly chosen iid number is $1/(N+1)$. Indeed, we have $N+1$ random

numbers in total, so that the probability to randomly pick the smallest among them is $1/(N+1)$. (Moreover, there is no need for independence.) In our case, $N=2$ and hence, $q=1/3$ and

$$K_{break,eff} = \frac{2}{3}K_{break} + \frac{1}{3}\frac{K_{break}}{\pi_{break}}. \tag{3}$$

We futher argue in Appendix A that in fact $1/3 < q < 1$. Because of the occurrence of the seam shift, it is impossible to have $q=1$. Hence, it is interesting to observe that *the seam shift may facilitate catastrophe by preventing the lock-up of the MT tip in a too stable perfectly blunt configuration*.

The simplest mean-field approximation would be to set for any i $p_i(t) = p(t)$ and $b_i(t) = b(t)$. Defining the "crack depth" $d(t) = p(t) - b(t)$ and always assuming that $b(t) \geq 1$,

$$\begin{cases} v_b(t) \equiv \dot{b}(t) &= -K_{break,eff} + K_{bond}H(d(t) \geq 1) \\ v_p(t) \equiv \dot{p}(t) &= K_{grow} - K_{shorten}d(t)(d(t)+1)/2 \end{cases}, \tag{4}$$

where we introduced mean-field bond and protofilament velocities v_b and v_p. However, given the mean-field nature of the approximation, it seems reasonable to modify the first equation to

$$v_b(t) \equiv \dot{b}(t) = -K_{break,eff} + K_{bond}(1-e^{-d}), \tag{5}$$

as $d(t)$ stands for the average crack depth. Individual lateral bonds may form even when $d(t) < 1$, and when $d(t) > 1$, not all the bonds have to be cracked. Indeed, assume that the individual cracks d_i are approximately Poisson-distributed with the mean depth d. Bonding can happen only if $d_i \geq 1$ and so $\langle K_{bond}\rangle = K_{bond}\mathrm{Prob}[d_i \geq 1] \approx K_{bond}(1-e^{-d})$. If we wish to approximate it by a second-order polynomial, the expression $\langle K_{bond}\rangle = K_{bond}d(1-d/4)$ for $d \leq 2$ (and $\langle K_{bond}\rangle = K_{bond}$ for $d \geq 2$) is a C^1 approximation of $K_{bond}(1-e^{-d})$.

We are interested in obtaining a steady-state behavior $v_p = v_b$, which would presumably describe either a growth phase of GMPCPP-Tu-like MT with sufficient [Tu], or an MT shortening phase. At long times, the mean-field crack depth $d(t)$ reaches a steady state value d_∞, which can be found from $\dot{d}(t) \equiv v_p(t) - v_b(t) = 0$:

$$K_{shorten}d_\infty(d_\infty+1)/2 + K_{bond}(1-e^{-d_\infty}) = K_{grow} + K_{break,eff}. \tag{6}$$

Now that we know the steady state crack depth d_∞, the velocity of MT length change (either growth or shortening) is given via the long-time asymptotics of $v_p(t) = v_b(t)$:

$$v_\infty = K_{grow} - K_{shorten}d_\infty(d_\infty+1)/2 = K_{bond}(1-e^{-d_\infty}) - K_{break,eff}. \tag{7}$$

Positive v_∞ means growth, negative means shortening. This equation determines the steady state velocity v_∞ of a one-dimer-type MT as a function of dimer-scale parameters and [Tu], which affects K_{grow}. Based on derivations above, we see that there is always a solution, and this solution is unique (because both terms on the left of eq. 6 are increasing functions of d_∞, while the right is constant). In other words, a single dimer type MT under constant external conditions will either grow to infinity or shorten to zero. As expected, there is no dynamic instability. The situation becomes more diverse when we introduce hydrolysis in Section III B below.

From eq.(7), we see that when K_{grow} decreases, so does d_∞, and eventually, v_∞ will become negative. Also, if the parameters are such that $K_{bond} < K_{break,eff}$, then MT growth is not possible, no matter how large [Tu] is. This simply states that the lateral bonds are energetically unfavorable, so the neighboring protofilaments will not bond together.

To estimate the depolymerization (shortening) velocity, we can put $K_{grow} = 0$ (or a sufficiently small value), because shortening velocity is roughly independent of [Tu] for GDP-Tu MT. Also, all the rates should correspond to the considered dimer type (e.g., should use rates for GTP-Tu (GDP-Tu) for regular growing (shortening) MT). See Appendix C for more details.

B. Model with hydrolysis

We now relax the restriction that all the dimers must be identical. The GTP-Tu dimers can hydrolyze with hydrolysis rate K_h to the GDP-Tu, making the MT less stable. We assume here that, as in the discussed numerical simulations, the identity of the dimer (either GTP or GDP) affects only the lateral breakage rates. Dependence of shortening, growth, and/or lateral bonding on dimer identity can be accommodated along the lines presented below.

As we are using a mean-field approach, we want to estimate the effective lateral breakage rate that will now depend on the age of the dimer; the older it is, the higher the chance that it is a GDP-Tu dimer and consequently, the higher the breakage rate. If the

MT grows, then, given the dimer age t, the probability not to hydrolyze by this age is $\eta = e^{-tK_h}$. When the MT is shortening, then one should assume $\eta = 0$, as the dimers that get exposed at the MT tip had stayed in the MT lattice for a long time. The breakage rate depends on the identities of two laterally neighboring dimers, and hence

$$K_{break,eff} = \eta^2 K^{TT}_{break,eff} + \eta(1-\eta)[K^{TD}_{break,eff} + K^{DT}_{break,eff}] + (1-\eta)^2 K^{DD}_{break,eff}, \tag{8}$$

where the superscripts stand for the corresponding neighbors, and each of $K^{XY}_{break,eff}$ can be calculated as in (3). The rest is similar to the treatment of Section III A, and the only open issue is how to determine the age t, when the MT is growing. To answer this, we recall that in the case of a one-dimensional random walker, the distribution of its first passage times over distance x is given by $f(t;x) = \frac{|x|}{\sqrt{4\pi D t^3}} \exp\left(-\frac{(x-vt)^2}{4Dt}\right)$ with the mean first passage time x/v in the direction of average drift. (This last relation should be obvious as this is in fact the meaning of the average velocity v.) Hence, we can say that the visit to the position of origin was time x/v ago (on average), if the walker has just arrived at a location at distance x from the origin (and the current position has age zero). In our case, velocity v (the average drift of the tip of a protofilament) is not constant and depends on the crack depth x. Therefore, the mean age of the dimer sitting just at the bottom of the crack (at the depth d from the MT tip) can be approximated as

$$\langle t \rangle = \int_0^d \frac{dx}{v(x)} = \int_0^d \frac{dx}{K_{grow} - x(x+1)K_{shorten}/2} = \frac{2}{\gamma K_{shorten}} \ln\left|\frac{1+2d/(\gamma+1)}{1-2d/(\gamma-1)}\right|, \tag{9}$$

where $\gamma = \sqrt{1+8K_{grow}/K_{shorten}}$ and we have used the expression (4) for the protofilament growth velocity as a function of crack depth. Note that $\langle t \rangle$ logarithmically diverges when the steady-state MT growth velocity $v(d)$ approaches zero. We also observe that when $v(d) = 0$, then $d = d_{cusp} = (\gamma-1)/2$, and $\langle t \rangle$ given by (9) is infinite. Given that shortening events can happen everywhere in the cracked region, one could wonder if $\langle t \rangle < 1/K_{shorten}$, where $1/K_{shorten}$ is the mean life time of the longitudinal bond, in the absence of lateral bonds. The equation $\langle t \rangle < 1/K_{shorten}$ leads to $d < d_0 \equiv (e^{\gamma/2}-1)/\left(2\left(1/(\gamma+1) + e^{\gamma/2}/(\gamma-1)\right)\right)$, and the ratio $d_0/d_{cusp} = 1 - 2\gamma/\left((\gamma+1)e^{\gamma/2} + \gamma - 1\right)$ is close to 1 for large enough γ. For $\gamma = 1$, $d_0/d_{cusp} \approx 0.39$, while for $\gamma = 3$, $d_0/d_{cusp} \approx 0.70$, and for $\gamma = 5$, $d_0/d_{cusp} \approx 0.87$. Respective values of d_{cusp} are 0, 1 and 2.

The age of dimers n dimer lengths below the crack should be estimated as $\langle t \rangle + n/v_g$ (if they polymerized during the current growth phase), where $v_g = v(d_g)$ is the growth velocity and $d = d_g$ is the crack depth at the growth phase. Therefore, we can estimate a laterally bonded GTP-Tu cap length (the number of GTP-Tu dimers below the crack), ℓ_b, from the relation $1/K_h \approx \langle t \rangle + \ell_b/v_g$, yielding at steady state

$$\ell_b \approx v_g(1/K_h - \langle t \rangle). \tag{10}$$

For the growth to be possible, we need $\langle t \rangle < 1/K_h$. The estimate of the total number of GTP-Tu in the MT body then would be $13 \cdot (\ell_b + d_g)$ for 13 protofilaments. See Appendix C for an additional discussion of (9).

To be precise, we would like to determine $\eta = \left\langle e^{-tK_h} \right\rangle$ with $\langle t \rangle$ given above. The two simplest choices would be either to assume $t = \langle t \rangle$ always, leading to $\eta = e^{-\langle t \rangle K_h}$, or to assume that t is exponentially distributed with mean $\langle t \rangle$, leading to

$$\eta = 1/(1 + \langle t \rangle K_h). \tag{11}$$

Both of these approximations lead to very similar results. We choose the latter one, as our numerical simulations (see Appendix C) indicate that, typically, distribution of t is close to the exponential.

As in Section III A, to find the steady-state solutions, we need to solve the equation $\dot{d}(t) \equiv \dot{p}(t) - \dot{b}(t) \equiv v_p(t) - v_b(t) = 0$, where now $K_{break,eff}$ is a function of d, through (8,9,11). This equation can be solved numerically.

In Figures 5 and 6, we plot $\dot{d} \equiv v_p - v_b$ as a function of d. Depending on [Tu], there is typically either one or three solutions to the steady state $v_p = v_b$, with the transient case of two solutions. Observe that the cusps (the local maxima) in these graphs occur when $\langle t \rangle$ from (9) reaches infinity, indicating that the dimers at both sides of the top lateral bond are GDP-Tu. However, this happens exactly when v_p drops to zero (see discussion after (9)). Note that v_p grows when d decreases (cf. (4)); hence, $v_p > 0$ to the left of the cusp, and $v_p < 0$ to the right of it. Since at the steady state $v_p = v_b = v_\infty$, it follows that at the steady-state $v_\infty > 0$, if the intersection of the considered curve with the abscissa is to the left of the cusp and vice versa. We denote the value of d at the cusp, for which $v_p(d) = 0$ by d_{cusp}.

There are several interesting features displayed in Figures 5 and 6. First, when [Tu] is low, there is only one solution for the steady state crack depth d_∞, and this solution has negative MT velocity ($v_\infty < 0$), i.e., there is no macroscopic polymerization possible. When [Tu] is large, there are three solutions for d_∞, which we denote d_g, d_u and d_s. The left and the right ones (d_g and d_s, respectively) are stable solutions and correspond to the MT growth and shortening phases. The middle solution, d_u, is unstable and is therefore transient. (The stability of a solution is determined by slightly perturbing the steady state value. If a small increase in d from its steady state value d_∞ leads to negative $\dot{d} \equiv v_p - v_b$, then d will decrease and return to d_∞, which is

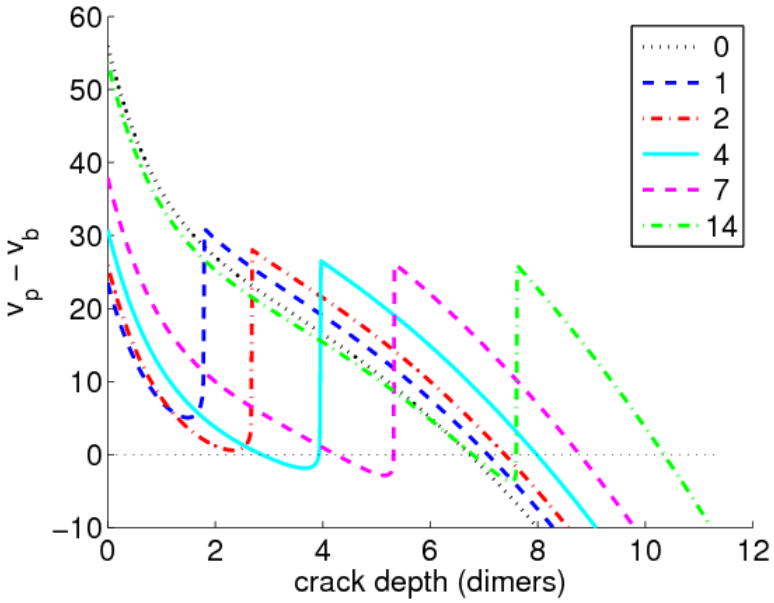

Figure 5: (Color online) Dependence of $\dot{d} \equiv v_p - v_b$ on the crack depth d for the set 3m. The steady state solutions are found when $v_p - v_b = 0$. Legend denotes free GTP-Tu concentrations, [Tu], in μM. When [Tu] is sufficiently high (above $2\mu M$), there are three steady state solutions for each curve. The left and the rightmost, denoted in the text as d_g and d_s, are stable growth and shortening solutions, respectively, because the slope of the curve is negative. The middle solution, d_u, is an unstable "pause" solution, whose velocity is just slightly positive. See text for details.

then a stable solution. If, on the other hand, a small increase in d leads to positive $\dot{d} \equiv v_p - v_b$, then d will increase even further, so that such a solution is unstable.) One could argue that the middle solution represents the "pause" state, as discussed later. It is tempting to think of a difference $d_u - d_g$ as the length of the laterally bonded GTP cap. However, this does not have to be true, as d_u reflects the crack depth after the loss of some dimers from the protofilament tip, in order to accommodate for the drop in v_b. So, $d_u - d_g$ should be smaller than the laterally bonded GTP cap length. We note that, depending on parameters, only the steady-state growth solution could be possible, when the cusped maximum between d_u and d_s would fall below the $\dot{d} = 0$ line. An extreme example of that situation is when GDP-Tu dimers are identical to GTP-Tu dimers. We also observe that under given assumptions, $d_s > d_g$ always, for a fixed [Tu].

Figures 7 and 8 show the steady-state crack depth and MT velocity as functions of [Tu]. The shortening velocity is overestimated in comparison with numerical simulations by a factor of 2 to 3; compare this to Figures 3 and 4. This discrepancy can be explained by our choice of $q = 1/3$, while all bond heights can have a very limited choice of values (at any given time), so that q should be higher (see Section III A after (3)). We also see that the theoretical estimates of the crack depths are close to the values of d and Δ given in Table I. Slightly higher theoretical estimates of d_s are again explained by our choice of $q = 1/3$, which leads to overestimation of v_s and hence overestimation of d_s as well. Using (10), the theoretical estimates for the number of GTP-Tu dimers and of the laterally bonded cap length for the concentrations listed in Table I are 467 and 29 for set 3m and 61 and 3.3 for set S8, respectively. If, instead of comparing values for a given [Tu], we use similar v_g then for set S8, we take theoretical estimates when [Tu]$= 12\mu M$, which lead to 118 GTP-Tu dimers and laterally bonded cap length of 7.5 dimers.

There are two additional observations. First, the velocity at pause v_u is just slightly above zero because d_u is just slightly below d_{cusp}, which is the position of the cusp maxima at which $v_p(d_{cusp}) = 0$. This provides justification for calling this state a "pause" (see also [15, 17]). Second, the curvature around the local minima between $d = 0$ and $d = d_{cusp}$ determines the initial polymerization velocity when it first becomes possible (when the minimum touches the $v_p - v_b = 0$ line). The steeper the curve, the closer the initial v_g to zero. This happens for the same reason as above, namely, when the minimum touches the $v_p - v_b = 0$ line, formally $d_g = d_u \lesssim d_{cusp}$. This observation describes initial appearance of the growth steady state.

The curves in Figures 5 and 6 should be treated with care. They are perfectly justified, given the nature of discussed approximations, only at and near the steady state $\dot{d} \equiv v_p - v_b = 0$ line. Beyond the vicinity of the steady state, the system, even under the current approximations, cannot be solely described by a single parameter d. This situation is analogous to consideration of a physical system at equilibrium and fluctuations around it. When the fluctuations are small, equilibrium statistical mechanics is still valid, and the state of the system can still be described by a few relevant macroscopic parameters. When the system is far from equilibrium, this approach is no longer valid. In our case, it matters whether the change in v_b or in v_p or the change in both of them caused a change in the steady-state value of d. Depending on this, the consequent decay in this fluctuation will follow

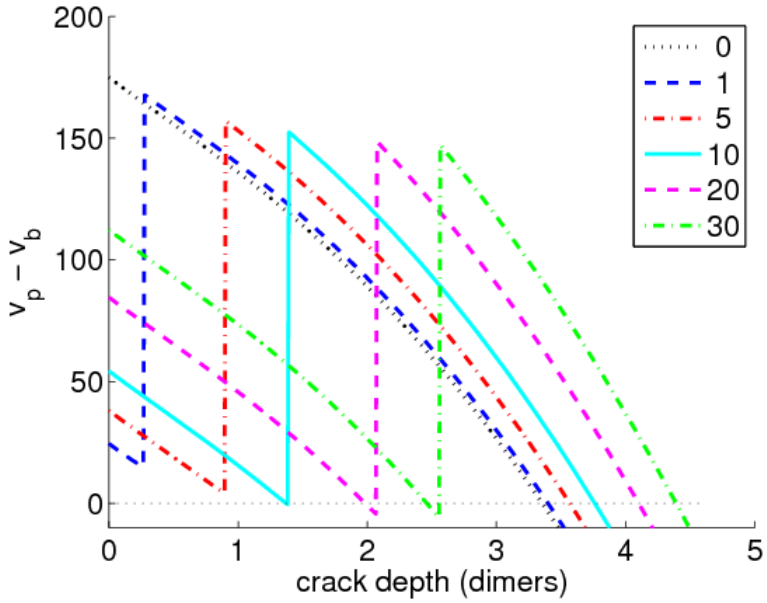

Figure 6: (Color online) Dependence of $\dot{d} \equiv v_p - v_b$ on the crack depth d for the set S8. Legend denotes free GTP-Tu concentrations, [Tu], in μM.

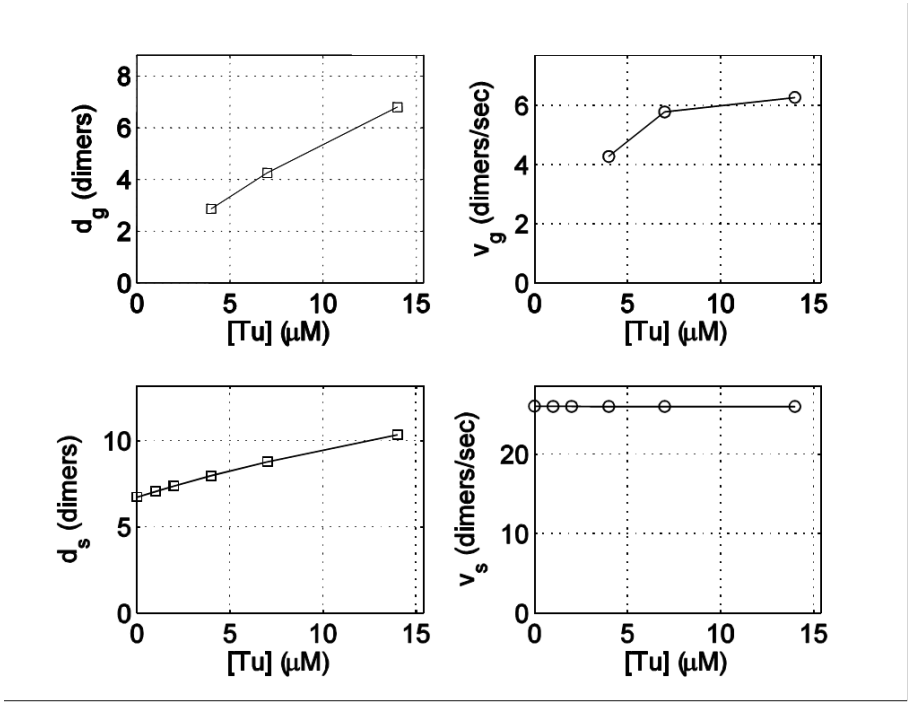

Figure 7: Crack depth (squares) and growth and shortening velocities (circles) as functions of [Tu] for set 3m. For small [Tu], there is no growth solution, so no data are shown.

different curves, leading to a hysteresis-like picture (see Figure 9). In Figure 9, the upper and the lower dotted curves represent the one-dimer-type GDP-Tu and GTP-Tu microtubules described at the end of Section III A, reflecting shortening and growth, respectively.

While our MFM deals quantitatively with steady states, we can still think in its terms, in order to qualitatively describe conceivable ways of the phase transitions. For the catastrophe to happen, there should be a significant fluctuation in the crack depth, causing it to penetrate into the GDP-rich inner part of the MT. The v_b should decrease in this case. As the minimum of

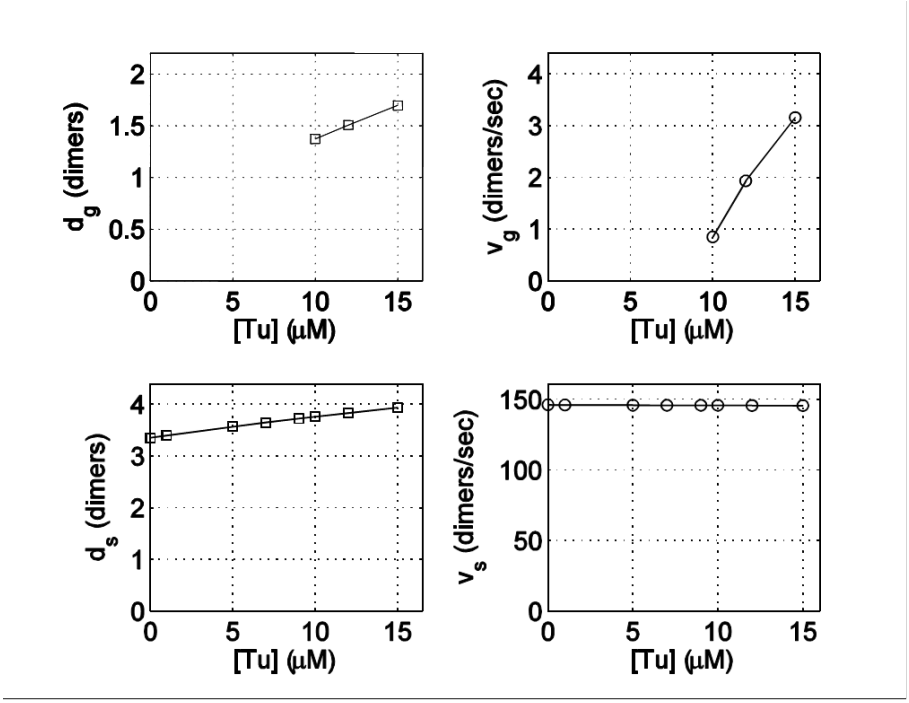

Figure 8: Crack depth (squares) and growth and shortening velocities (circles) as functions of [Tu] for set S8. For small [Tu], there is no growth solution, so no data are shown.

$\dot{d} \equiv v_p - v_b$ between d_g and d_u becomes deeper with [Tu], the frequency of catastrophe should go down (see Figures 5, 6 and Appendix D). For the rescue to happen, the crack should become very short or disappear altogether, starting from the steady-state value d_s and following the upper dotted line of Figure 9. Note that these fluctuations are independent of [Tu], and hence on the height of the cusped maximum in $v_p - v_b$, as the shortening can happen independently anywhere along the laterally unbonded part of the protofilament (i.e., anywhere in the crack region). Then, if there is a sufficient supply of soluble GTP-Tu (i.e., [Tu] is large enough), rescue becomes likely when the newly polymerized GTP-Tu dimers form lateral bonds. In terms of our model, this would mean the transition from the upper dotted line to the lower (full) line somewhere around small d values. The higher the [Tu], the more likely the rescue is to happen, as opposed to the relaxation back to the shortening steady-state depth d_s. One could expect that the frequency of switching to the lower curve is proportional to $P_{0,s}K_{grow}$, where $P_{0,s}$ is the probability to have zero crack depth in the shortening phase (cf. Appendix C; another possibility would be to use $K_{shorten}\left[K_{grow}/(K_{grow}+K^{DD}_{break,eff})\right]$ or similar expressions, which is proportional to [Tu] when it is not too high. Indeed, the total rate of a step (any event) in the shortening phase can be approximated as $K_{tot} = K^{DD}_{break,eff} + K_{bond}(1-P_0) + K_{grow} + K_{shorten}d(d+1)/2$. Let us assume that we first need to obtain a zero crack depth, with probability $K_{shorten}/K_{tot}$, and then to add a GTP-Tu before developing a crack, with probability $K_{grow}/(K_{grow}+K^{DD}_{break,eff})$. If these two events are what is needed in order to switch to the lower curve, then we have to multiply K_{tot} by these two probabilities). For the multi-protofilament MT, however, these arguments can hardly count as a good approximation, as different protofilaments and bonds do not act synchronously during the phase transitions.

Emergence of growth solution and of the unstable "pause" between growth and shortening bears close resemblance to the formal Landau theory of phase transitions [33]. For example, Sept and Tuszynski [34] use this theory to describe co-existence of free tubulin and assembled MTs. However, there are significant differences as well. Unlike [34], our approach is directly based on the dimer-scale model parameters, and we are able to predict steady-state characteristics of the MT growth. In addition, the Landau-Ginzburg model yields that for high enough [Tu] the coexistence of free and polymerized tubulin is impossible. This would correspond to unbounded MT growth. What we have does not contradict this obviously correct result but is somewhat different: we always have a shortening solution. There is a well-known concept of multistability in biological systems [35], and we have a bistable system. However, as the catastrophes become very rare and rescues frequent, the shortening phases, while theoretically possible, will not be clearly distinguishable (see Appendix D).

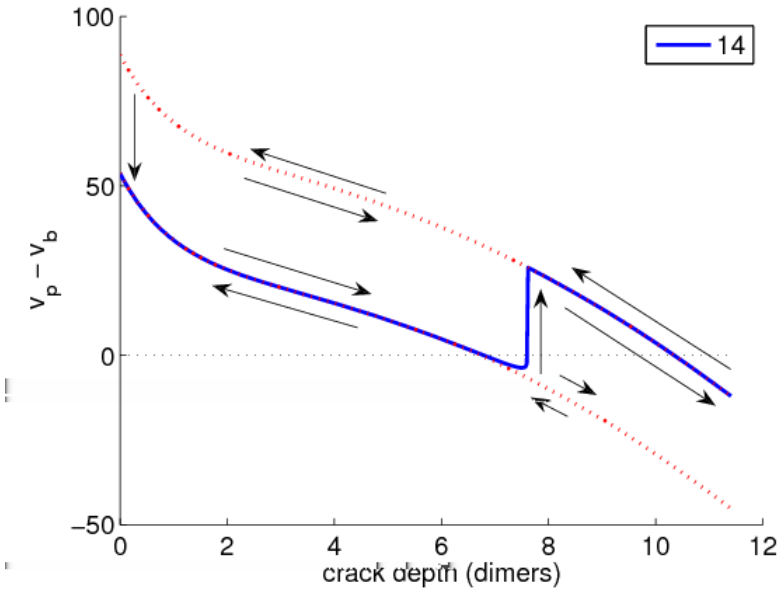

Figure 9: (Color online) Dependence of $\dot{d} \equiv v_p - v_b$ on the crack depth d for the set 3m for [Tu]$= 14\mu M$. Depending on the cause of the fluctuation in the steady-state value of d, its subsequent relaxation can follow either the blue or the red lines, and the transition from upper to lower curve and vice versa does not necessarily have to occur along the vertical blue connection. Arrows schematically show fluctuations in d and transitions between growth (lower curve) and shortening (upper curve) phases.

IV. CONCLUSIONS

There are multiple studies of microtubules (MTs) and their dynamic instability (DI). Many papers focus on modeling DI and its consequences by using simplified representation of MTs in the form of linear fibers and introducing DI parameters. Other papers aim to explain and/or justify some of these parameters by considering MT structure in more detail. Computational dimer-scale lattice and mechanochemical models have been developed to this end. There are also theoretical models addressing the catastrophe frequency and growth. However, the quantitative theoretical understanding of the computational models and of MTs themselves at a scale of inter-dimer interactions remains limited. The most conspicuous feature missing from the theoretical and from majority of the computational approaches is the explicit consideration of interprotofilament interactions that would allow for cracks.

In this paper, a dimer-scale numerical Monte Carlo model of MT dynamics, which takes experimental observations of inter-protofilament cracks into account, was constructed. Two different parameter sets were used to demonstrate the model's behavior, both displaying dynamic instability at certain tubulin concentrations [Tu], similar to experimental observations. Dynamic instability was quantified using the standard four parameters: velocities of growth and shortening phases and frequencies of the phase transitions. In addition, the GTP-cap characteristics and the crack depths have been determined.

Next, a theoretical dimer-scale mean-field model (MFM) was introduced near the steady-state. Predictions obtained using this model were compared with the Monte Carlo simulations for the same values of parameters. In spite of many simplifying assumptions used in the derivation of the MFM, its predictions were shown to be in good agreement with the Monte Carlo simulations. As a result, a connection was established between dimer-scale processes and macroscopic characteristics of MT dynamics.

The MFM was used to predict the minimal concentration of free tubulin needed for polymerization. It also predicted existence of the growth, shortening and pause states, and it was used for calculating their respective velocities. The MT tip structure was also described in terms of crack depths and a laterally bonded GTP-Tu cap length. The original idea of [7] to use a two-state approach to MT dynamic instability was elaborated and a more detailed picture of dynamic instability cycle was presented (Figure 9).

More specifically, the model analysis yielded that for sufficiently high [Tu] and with hydrolysis taking place, there existed stable growth and shortening states, as well as an unstable "pause" state. These states are caused by the interplay of longitudinal (within-protofilament) and lateral (between-protofilament) dimer interactions.

Also, the model predicted that there was no growth steady state for low [Tu]. This is stronger than just saying that the MT would grow at small [Tu] but stay short. There is a discontinuous transition meaning that there appears a growth steady state at some positive $[\mathrm{Tu}]_\mathrm{C}$. Below this $[\mathrm{Tu}]_\mathrm{C}$, the steady state growth phase does not exist, and the MT cannot grow.

The MFM described in Section III is a novel theoretical-mathematical quantitative framework describing steady states of an MT-like polymer consisting of multiple laterally connected protofilaments/strands. Howard [37] discusses the stability of two-stranded polymer versus one-stranded and shows that the former is long, while the latter is short. All one-dimensional (linear or one-stranded) models simply have to postulate/imply that the fiber/protofilament cannot break anywhere in the middle. Hence, effectively, these models cannot be represented at dimer-scale. On the other hand, our model cannot be reduced to a one-dimensional model because both protofilaments and bonds (i.e., their lateral interactions) are explicitly represented. We are able to devise a dimer-scale theory by making it two-dimensional.

Since we restricted our theory to the case when the depolymerization rate is not a function of the dimer identity, we presented in this paper only simulation results for such parameter sets. It is worth mentioning, however, that other simulations not subject to this restriction will be published in a forthcoming paper. Those results address certain experimental findings and yield interesting biologically important conclusions, but they are not of major interest for the current discussion.

Acknowledgments

This work was supported by grants NIH GM065420 and NSF MCB 0951264. We also thank Trevor Cickovski and Ivan Gregoretti for their contributions in developing the computational model code.

Appendix A: Processes taking place in the model

The model simulates the events occurring in a 13-protofilament microtubule at the dimer scale. It includes five processes: protofilament growth, protofilament shortening, inter-protofilament bond growth, inter-protofilament bond shortening, and the transition of each GTP-Tu subunit to GDP-Tu (i.e. GTPase). At each step, the algorithm checks all possible events that can occur in any of the protofilaments and bonds and determines the fastest event. This event is then implemented. After that, the hydrolysis cycle is run, randomly converting GTP-Tu dimers into GDP-Tu dimers. Then, the next step begins.

Growth is the addition of a single subunit (single tubulin heterodimer) from the solution to the end of a protofilament. The probability of growth depends on soluble tubulin concentration and the identity (i.e., GTP/GDP) of the dimer at the tip. *Shortening* is a depolymerization event that is independent of soluble tubulin concentration. Instead, it depends on the presence/absence of lateral bonds between subunits, which are influenced by the nucleotide states of the subunits in question. Any part of a laterally unbonded protofilament end can detach, meaning that multiple subunits can fall off simultaneously, which is consistent with experimental observation [36]. *Bonding* is the formation of a new lateral bond between two dimers of neighboring protofilaments. A new lateral bond can form only if the subunits below it are already laterally bonded (similar to a zipper). This is reasonable given the likely separation between unbonded protofilaments. *Breaking* is the loss of such a bond. An existing bond can break only if it is the highest (last) bond between the two protofilaments. (This rule is based on the structural constraints inside the MT lattice.) The bonding and breaking rules result in the formation of continuous bonded segments between protofilaments from the seed up to the point at which a crack between protofilaments starts. *Hydrolysis* is modeled as a stochastic first order process. Hydrolysis can occur only in interior subunits (not on the terminal subunit of a protofilament), which is consistent with structural data indicating that binding of alpha tubulin is necessary to induce the beta tubulin GTPase [36]. In the present version of the model the rate of hydrolysis is not influenced by the state of surrounding subunits.

The rate k_i of each possible event is calculated based on the identities of the neighboring dimers, except in the case of growth, where it also depends on soluble tubulin concentration. All rates are provided in the configuration file. We model the events as Poisson processes with waiting times following an exponential distribution. Then, the time for each event is drawn from its respective rate: $t_i = -\ln r/k_i$, where r is a random number uniformly distributed between 0 and 1. If this time is shorter than the previous shortest time, the present event becomes the candidate for implementation.

The rate of bond breaking depends on whether there are neighboring bonds at the same height. Effectively, this keeps MT shortening somewhat coordinated after catastrophe, so that it shortens roughly simultaneously along all the protofilaments. This dependence is justified by arguing that the steric constraints of being in the middle of a tight lattice make it harder for a dimer to break free (see also [23]).

Processes occurring on the protofilaments next to the seam are governed by different rates because the MT structure near the seam differs from that in the rest of the MT. Also, for the presently considered half-integer seam shift of 1.5 dimers, the bonds at the seam grow and shorten by half a dimer, in contrast to other bonds that evolve by a full dimer length. This is done to avoid introducing artificial asymmetry at the seam.

We now turn to eq.(3). Here is an alternative derivation of q. Let X,Y,Z be iid bond heights with some distribution function F; Y is the bond between X and Z. Conditioning on the value of $Y = y$, we want to find $q(y) = \text{Prob}[X \geq y \bigcap Z \geq y] = (\text{Prob}[X \geq y])^2 = (1-F(y))^2 = (G(y))^2$, where $G = 1-F$. Now, $q = \int_{-\infty}^{\infty} dF(y)q(y) = \int_0^1 G^2 dG = 1/3$. In fact, X,Y,Z are not independent, but this is not necessary for the derivation, as long as the joint probability (or density)

	K_h	k_+	$K_{shorten}$	K_{bond}	$K_{bond,seam}$	K_{break}	$K_{break,seam}$	π_{break}
3m	0.2	2.5	1	30	60	30, $T\|T$ 40, $T\|D$ 80, $D\|T$ 80, $D\|D$	60, $T\|T$ 150, $T\|D$ 150, $D\|T$ 150, $D\|D$	10
S8	0.25	3.5	20	30	60	30, $T\|T$ 40, $T\|D$ 40, $D\|T$ 250, $D\|D$	60, $T\|T$ 80, $T\|D$ 80, $D\|T$ 500, $D\|D$	1000

Table II: Parameter summary for sets 3m and S8. T stands for GTP-Tu and D for GDP-Tu. Lateral bond breakage rate K_{break} depends on the left and right neighbor, and its values are given for the specified neighbors $left|right$.

	ΔG^*_{long}, k_BT	ΔG_{lat}, k_BT	ΔG^{π}_{lat}, k_BT
3m	-14.7 (-6.2)	0, $T\|T$ 0.3, $T\|D$ 1, $D\|T$ 1, $D\|D$	-2.3, $T\|T$ -2, $T\|D$ -1.3, $D\|T$ -1.3, $D\|D$
S8	-12.1 (-3.6)	0, $T\|T$ 0.3, $T\|D$ 0.3, $D\|T$ 2, $D\|D$	-6.9, $T\|T$ -6.6, $T\|D$ -6.6, $D\|T$ -4.8, $D\|D$

Table III: Energies of regular bonds.

$P(X \geq x, Y = y, Z \geq z) = f(x,y)f(y,z)$, i.e., it splits into a product for any given y. Then the above derivation holds: $P(X \geq Y, Y = y, Z \geq Y) = P(X \geq Y, Z \geq Y | Y = y)P(Y = y) = P(X \geq y)P(Z \geq y)P(Y = y)$.

In fact, $q = 1/3$ is the lower estimate of q. In the case of discrete random variables (bond heights), q will be $\geq 1/3$ if there is a positive probability of having bonds of equal height. An extreme example is when all heights have to be identical: then, obviously, $q = 1$. Generally, for bond heights X, Y, Z we will have $q = P(X \geq Y, Z \geq Y) = \frac{1}{3}P(X \neq Y, X \neq Z, Y \neq Z) + \frac{1}{2}P(X = Y \neq Z \bigcup X = Z \neq Y \bigcup X \neq Y = Z) + 1P(X = Y = Z) \geq 1/3$, where $1/3$ arises as before, and $1/2$ occurs because (first) three out of the following six choices satisfy $\{X \geq Y, Z \geq Y\}$: $X = Y < Z, X > Y = Z, X = Z > Y, X = Y > Z, X < Y = Z, X = Z < Y$, and from the symmetry of the problem, the probability of the first three choices is equal to the probability of the last three. Because of the occurrence of the seam shift, it is impossible to have all 13 bonds at the same level simultaneously, so that $P(X = Y = Z) < 1$, making it impossible to have $q = 1$.

Appendix B: Parameter sets 3m and S8

Table II contains the parameters used in sets 3m and S8 described in this paper. Arbitrary units of time (aut) are used. For comparison to the experiment, 1aut $\approx$ 1sec. Respectively, K_h, $K_{shorten}$, K_{bond}, K_{break}, etc. are the rates of dimer hydrolysis, shortening (breaking the longitudinal bond), forming, and breaking the lateral bond (given in $(\text{aut})^{-1}$). The polymerization rate of a dimer is formally defined by the relationship $K_{grow} = (1/(k_+c) + 1/\kappa)^{-1} = \kappa\frac{c}{c + c_{1/2}}$, where c is the free tubulin concentration, κ is the maximal possible growth rate and $c_{1/2} = \kappa/k_+$ is the concentration at half-maximum. This relationship was chosen because it allows the reaction to saturate at infinite tubulin concentration. However, for all simulations in our analysis, the polymerization rate is governed by the more familiar relationship for a first order chemical reaction, i.e., $K_{grow} \approx k_+c$. This occurs because the equation for K_{grow} reduces to $K_{grow} = k_+c$ when $c \ll c_{1/2}$, and in both parameters sets, $c_{1/2} = 200\mu M$.

As the seam bond evolves by half-dimer (i.e., monomer) steps (in contrast to the regular bonds which evolve by full dimers), the seam lateral bonding and breakage rates are typically twice those of the regular bonds, for simplicity. The rate of breaking any lateral bond decreases by a factor of π_{break} if there are two presently formed lateral bonds to the left and to the right of the considered one.

The bond energy values of Table III are qualitatively similar to those used in [4, 17] and estimated in [3]. The authors of [18] cite values similar to [4, 17]. Note that the curvature energy $E_c(> 0)$ in [18] for straight GDP-Tu protofilaments is reflected in

our parameters through the decreased stability of lateral $D|D$ bonds in comparison to $T|T$ bonds. These energies are calculated using $\Delta G^*_{long} = -k_BT \ln \frac{k_+ 10^6}{K_{shorten}}$, with k_+ in units of $\mu M^{-1}\text{aut}^{-1}$, $\Delta G_{lat} = -k_BT \ln \frac{K_{bond}}{K_{break}}$, and $\Delta G^{\pi}_{lat} = -k_BT \ln \frac{K_{bond}}{K_{break}/\pi_{break}}$. Note that ΔG^*_{long} includes entropic contribution, and ΔG^{π}_{lat} arises instead of ΔG_{lat}, due to steric constraints, when both of the lateral neighboring bonds exist. The value in brackets for ΔG^*_{long} is calculated using $\Delta G^*_{long} = -k_BT \ln \frac{\kappa}{K_{shorten}}$, where κ is the maximal possible value of K_{grow} at high [Tu]. It is worth mentioning that the energy values and rates used are only a convenient approximation. It is plausible that actual bond breakage and formation dynamics are faster than that described by the rates of Table II. This would mean that actual bond energies are smaller if we want to preserve the bonding/unbonding ("zipping/unzipping") velocity.

In [4], for the value of $k_+ = 2\mu M^{-1}s^{-1}$, the authors predict $\Delta G^*_{long} = -9.4k_BT$ and $\Delta G^{GTP}_{lat} = -3.2k_BT$, where we now added a superscript GTP to indicate that this was the estimation of the lateral energy for the simulations of MT growth. For the simulations of MT shortening, [4] find $\Delta G_{kink} = 2.1k_BT$ leading to $\Delta G^{GDP}_{lat} = \Delta G^{GTP}_{lat} + \Delta G_{kink} = -1.1k_BT$. The energies ΔG^{GTP}_{lat} and ΔG^{GDP}_{lat} can be interpreted in terms of our model as the lateral bond energies between two GTP-Tu dimers (i.e., for $T|T$) and between two GDP-Tu dimers ($D|D$), respectively, and when all the *possible* lateral neighbor bonds exist (because in [4], there is no possibility of having broken bonds). There is also no lateral asymmetry in [4]. The structural computational studies [3] estimate that $\Delta G_{long} - \Delta G_{lat} \approx -7\text{kkal/mol} \approx -11.7k_BT$ for room temperature, which is also in agreement with our parameters.

Appendix C: Distribution of crack depths

Here, we make a more detailed analysis of the evolution of a crack depth, in comparison to Section III A. We denote P_i as the probability that the crack has a depth i. (Don't confuse this with p_i used in Section III A.) We have the following equations:

$$\dot{P}_0 = -K_{grow}P_0 + K_{shorten}\left(\sum_{j=1}^{\infty} P_j\right) + K_{bond}P_1 \tag{C1}$$

$$\dot{P}_i = -(K_{grow} + iK_{shorten} + K_{bond})P_i + K_{shorten}\left(\sum_{j=i+1}^{\infty} P_j\right) + K_{grow}P_{i-1} + K_{bond}P_{i+1} \quad \text{for } i \geq 1. \tag{C2}$$

It can be verified that $\sum_{i=0}^{\infty} \dot{P}_i = 0$. Note that we did not introduce any breakage rate. It, however, can trivially be added to the above equations by replacing K_{grow} with $K_{grow} + K_{break,eff}$.

To solve these equations, it is convenient to define

$$G_j = \sum_{i=j}^{\infty} P_i. \tag{C3}$$

We have the normalization (boundary) condition $G_0 = 1$; hence, $\dot{G}_0 = 0$ and for $j \geq 1$

$$\dot{G}_j = -(K_{grow} + K_{bond} + jK_{shorten})G_j + K_{grow}G_{j-1} + K_{bond}G_{j+1}. \tag{C4}$$

Our second boundary condition is of course the convergence of the series $\sum_{j=0}^{\infty} P_j$, which is equivalent to demanding $G_j \to 0$ as $j \to \infty$. If we want to stick to the discrete case, (C4) can be solved in Laplace space or for a steady state as follows. Let $\alpha = K_{bond}/K_{grow}$ and $\beta = K_{shorten}/K_{grow}$. Then, at steady state, we have a tridiagonal infinite system of linear equations $G_{j-1} - (1 + \alpha + j\beta)G_j + \alpha G_{j+1} = 0$ with unknowns G_1, G_2, ... and we should utilize $G_0 = 1$. This system can be solved numerically to a desired precision after choosing j_{max}, such that $G_{j_{max}+1} = 0$, as an approximation for the second boundary condition. Alternatively, there is an iterative solution. Define $x_j = G_{j+1}/G_j$. Putting $G_{j_{max}+1} = 0$ is equivalent to $x_{j_{max}} = 0$, and we can iteratively find all $x_{j-1} = 1/(1 + \alpha + j\beta - \alpha x_j)$ going from $j = j_{max}$ down to 0. Having found $x_0 \equiv G_1$, we can go in the reverse direction and find all $G_j = x_{j-1}G_{j-1} = \prod_{i=0}^{j-1} x_i$. The continuous (in j) version of these equations was used for the cap model proposed in [9]. It leads to a second-order differential equation $[(1+\alpha)/2]G''(j) + (\alpha - 1)G'(j) - \beta jG(j) = 0$ (at steady state) with the Airy function Ai as a desired solution, which decays to zero as j goes to infinity: $G(j) = e^{j(1-\alpha)/(1+\alpha)}\text{Ai}\left[\left((1-\alpha)^2 + 2\beta(1+\alpha)j\right)/\left((2\beta)^{2/3}(1+\alpha)^{4/3}\right)\right]/\text{Ai}\left[(1-\alpha)^2/\left((2\beta)^{2/3}(1+\alpha)^{4/3}\right)\right]$.

It is easy to derive the moments of the crack depth distribution:

$$\langle i \rangle = \sum_{i=1}^{\infty} iP_i = \sum_{i=1}^{\infty} G_i \tag{C5}$$

and

$$\sum_{i=1}^{\infty} iG_i = \frac{1}{2}\left(\left\langle i^2\right\rangle + \langle i\rangle\right). \tag{C6}$$

Setting the average crack depth $d = \langle i\rangle$, from (C1,C2) or (C4) we can derive the following equation for the evolution of d:

$$\dot{d} = K_{grow} - K_{bond}G_1 - K_{shorten}\left(d + \left\langle i^2\right\rangle\right)/2. \tag{C7}$$

Observe that $G_1 = 1 - P_0$ is the probability that the crack depth is at least one dimer. In addition, if we have $P_i = \delta_{i,d}$, then $\left\langle i^2\right\rangle = \langle i\rangle^2 = d^2$ and (4) is recovered, after replacing K_{grow} with $K_{grow} + K_{break,eff}$.

We have performed simulations to check our analytical derivations and to estimate the age of a dimer when it becomes laterally bonded. In these simulations, we did not have lateral breakage events. The results are presented in Figure 10. The main conclusions from these simulations are that we have good mean-field estimates of the crack depth and of the dimer age at lateral bonding (or dimer age near the crack bottom) for a wide range of parameters. It is true that our mean-field age estimate (red lines in the left column) is too high for small K_{bond} because the mean age cannot go beyond $1/K_{shorten} = 1$. However, here we are dealing with a simplified situation of no lateral breakage. Allowing lateral breakage will permit ages above $1/K_{shorten} = 1$ because long-bonded dimers might become unbonded again. In that case, our mean-field formula should be even more accurate.

Appendix D: Catastrophe frequency

We now use a mesoscopic approach [8] to estimate catastrophe frequency. The idea is to assume that when the crack penetrates the GDP-Tu rich inner body of the MT, in analogy to the disappearance of a GTP-Tu cap in [8], this leads to a catastrophe. Only the lateally bonded part of the cap prevents catastrophe, and the length of this part fluctuates. In [8], a one-dimensional MT evolved by one-dimer steps. In the present model, the bond length serves as a good approximation of MT length, and it evolves by one-dimer steps as well. We let $K_{gT} = K_{bond}(1 - e^{-d})$ (see Appendix C) and $K_{sT} = K_{break,eff}$, where K_{gT} and K_{sT} stand for the rates of gaining and losing one dimer in the MT length (see [8]). Here, we only consider the case of growing MT; otherwise, there is no point talking about catastrophe.

Following the mesoscopic approach, we estimate the catastrophe frequency as

$$f_{cat} = K_{sT}^{eff}/n_{meso} \tag{D1}$$

where

$$K_{sT}^{eff} = \frac{-K_{gT} + K_{sT} + \sqrt{(K_{gT} - K_{sT})^2 + 4\beta_{meso}}}{2}, \tag{D2}$$

$$n_{meso} = \frac{K_{gT}K_{sT}}{K_{gT} + K_{sT}} \frac{\sqrt{(K_{gT} - K_{sT})^2 + 4\beta_{meso}}}{\beta_{meso}}, \tag{D3}$$

$$\beta_{meso} \equiv \frac{K_{gT}K_{sT}}{\tau + \rho \cdot \dfrac{K_{gT} + K_{sT}}{K_h}} \tag{D4}$$

and ρ is the auxiliary parameter such that $1/2 \le \rho \le 1$ (see [8]). We also use an additional parameter τ, which is the probability that the dimers at the level of the last formed bond cannot hydrolyze. In the original mesoscopic model, we assumed that the dimer at the very tip does not hydrolyze, corresponding to $\tau = 1$. Presently, we are concerned with bonds, and therefore $\tau = 0$ might be a better choice. Perhaps, a more accurate identification would be to use $\tau \sim P_0$, where P_0 is the probability of having zero crack depth (see Appendix C). Nevertheless, for the range of parameters used, this modification is negligible. An estimate of the laterally bonded cap length is $\ell_b \approx \tau + v_g(1/K_h - \langle t\rangle)$ - cf. (10).

Note that if penetration of only a single crack into the GDP-Tu rich MT is sufficient for the initiation of the catastrophe, then a better choice might be $K_{sT} = K_{break}/\pi_{break}$, i.e., $q = 1$, because this single crack will be the deepest one. Also, as we argued in Section III A, it is reasonable to have $q > 1/3$. The higher the q, the smaller the catastrophe frequency. In Figure 11, we show the theoretical estimates of f_c for the two parameter sets for different values of ρ and q. Unfortunately, the curves cover a wide range of possible values, so it is difficult to make any predictions. Nevertheless, the results of numerical simulations lie inside this range.

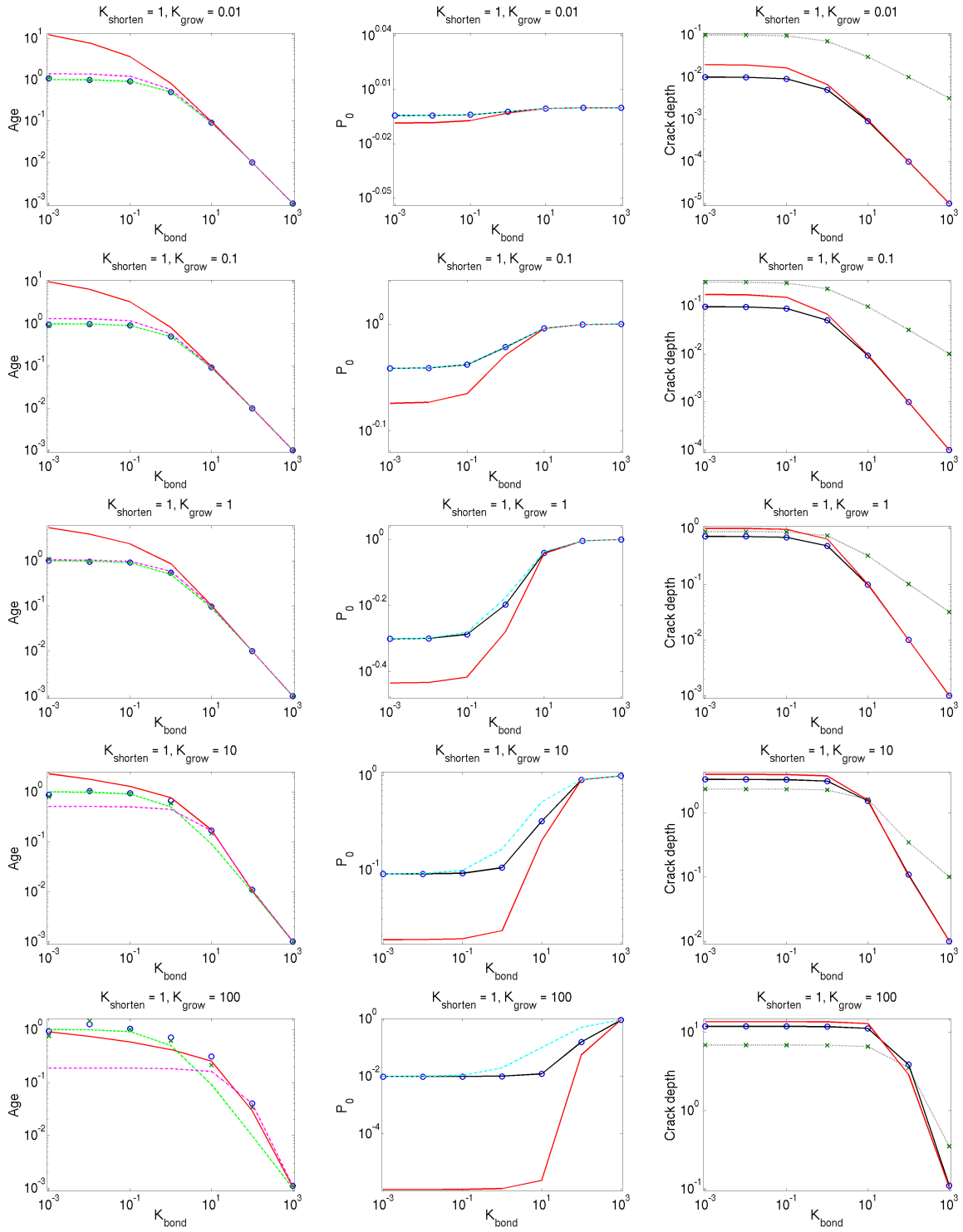

Figure 10: (Color online) Crack depth simulations of (C1,C2) for $K_{shorten} = 1$ and $K_{break} = 0$, and theoretical predictions. The columns from left to right show dimer age at a time of lateral bonding, probability of no crack P_0, and crack depth, as functions of K_{bond} with K_{grow} fixed. The rows from top to bottom correspond to $K_{grow} = 0.01, 0.1, 1, 10$ and 100, respectively. Blue circles are the means, and green crosses (on the left and right panels) are the standard deviations obtained from the numerical simulations. Full and dotted (on the right panels) black lines are the corresponding exact theoretical solutions described in the text, perfectly matching the simulations (circles and crosses). (We do not have exact solutions for the age.) Red full lines are the mean-field approximations: we assumed $P_0 = e^{-d}$ (see after eq.(4)) and numerically solved $K_{grow} - K_{shorten} d(d+1)/2 = K_{bond}(1-P_0)$ for d (cf. (7)). Then, for the age we used (9), and we plotted two additional estimates: the dashed green line is $1/(K_{bond} + K_{shorten})$, and the dash-dotted magenta line was calculated using (9), but now with the exact solution for d. The dash-dotted cyan line is an approximation for P_0 given by $\left[1 + K_{grow}/(K_{bond} + K_{shorten})\right]^{-1}$.

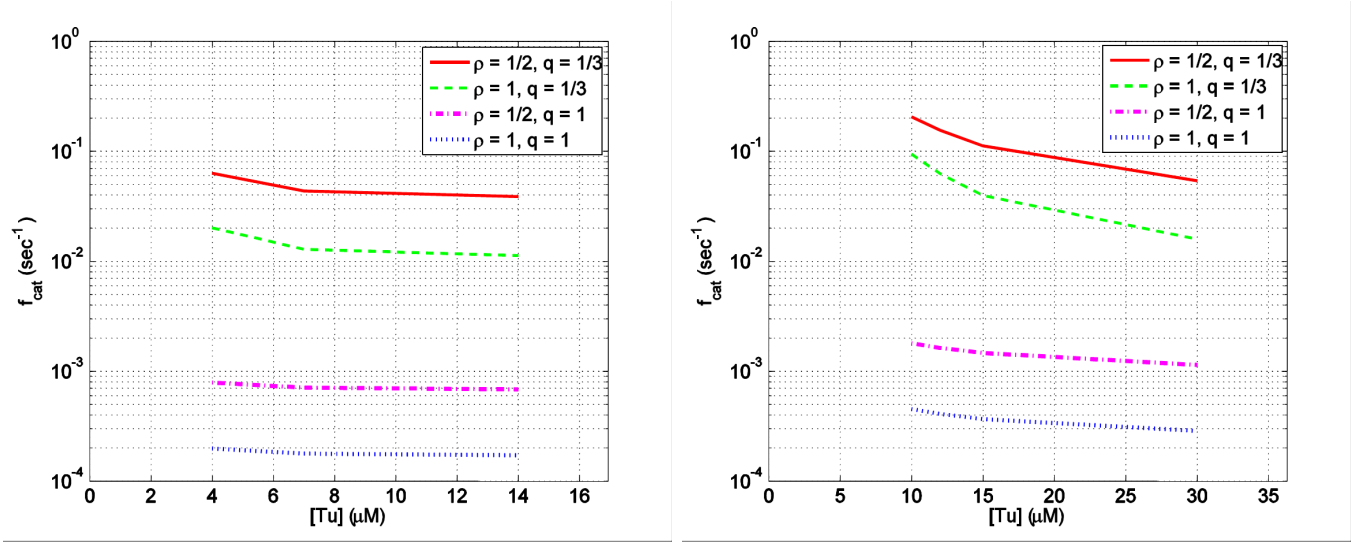

Figure 11: (Color online) Theoretical estimates of the frequency of catastrophe for sets 3m (left) and S8 (right) for different values of ρ and q.

We point out that in simulations and in experiments as well, selecting a threshold to determine phase transitions can effectively reduce the frequency of catastrophe if the rescue frequency is large and vice versa. This effect is not present in the theory. For example, ideally, the algorithmic threshold h for the decision to switch the phase should be $h \ll \lambda_g, \lambda_s$, where $\lambda_g \equiv v_g/f_c$ and $\lambda_s \equiv v_s/f_r$ are characteristic growth and shortening interval lengths. If the MT was growing but its length actually decreases by h, then we switch to the shortening phase, and vice versa. Also, h should not be too small in order to disregard fluctuations in length during a given phase. However, if $\lambda_g \ll \lambda_s$, it can be that $h \sim \lambda_g$ and then $f_r \approx f_{r,t} \exp(-f_{c,t}(h/v_g)) \approx f_{r,t} \exp(-h/\lambda_g)$, where the subscript t stands for theoretical estimates. So, if the rescue frequency is small, it may be significantly underestimated even more. Similar arguments apply when $\lambda_g \gg \lambda_s$. Note that the mean MT length λ satisfies $1/\lambda = 1/\lambda_g - 1/\lambda_s$ (e.g., [8]). When $\lambda < 0$, the MT growth is unbounded, and the transition from bounded to unbounded growth happens when $\lambda_g = \lambda_s$.

Alternative versions of the mesoscopic approach of [8] can be constructed. The idea still is to conserve the mean velocity and dispersion when rescaling the step from one-dimer-long to n-dimer-long. For example, as the waiting times between the steps are now exponentially distributed, we might use the formulas $v_{g,i} = i(\lambda_i - \mu_i)$ and $D_i = (\lambda_i + \mu_i)i^2/2$, where i defines the step length, and λ_i and μ_i denote (effective) rates of going up or down (with $\lambda_1 = K_{gT}$ and $\mu_1 = K_{sT}$). Then, we might solve the two equations $v_{g,1} = v_{g,n}, D_1 = D_n$ with $n = \tau + \rho(\ell_b - \tau)$, where μ_n would be the estimate of catastrophe frequency. The problem with this solution is that for n too large, it yields negative μ_n (if $\lambda_1 > \mu_1$). This means that for such n, it is impossible to have an upscaled (rescaled) evolution with exponentially distributed step durations. To overcome this limitation, we can replace D_n by the expression suitable for the fixed step duration (cf. [8]; we have a freedom to choose what the rescaled process will be): $D_n = 2n^2\lambda_n\mu_n/(\lambda_n + \mu_n)$. The solution is $\mu_n = \left((\mu_1 - \lambda_1) + [(\mu_1 + \lambda_1)/(2n)] + \sqrt{(\mu_1 - \lambda_1)^2 + [(\mu_1 + \lambda_1)/(2n)]^2}\right)/(2n)$. This estimate gives larger catastrophe frequencies than those in Figure 11. One can argue that it might be harder to catastrophe in the multi-protofilament MT than in the "mean-field" MT, so that the mean-field expressions tend to overestimate the true catastrophe frequency.

[1] T. Mitchison and M. Kirschner, Nature **312**, 237 (1984).
[2] S. S. Andersen, Bioessays **21**, 53 (1999).
[3] D. Sept, N. A. Baker and J. A. McCammon, Protein Sci. **12**, 2257 (2003).
[4] V. VanBuren, D. J. Odde and L. Cassimeris, Proc. Natl. Acad. Sci. USA **99**, 6035 (2002).
[5] A. Desai and T. J. Mitchison, Annu. Rev. Cell Dev. Biol. **13**, 83 (1997).
[6] A. V. Popov and E. Karsenti, Trends Cell Biol. **13**, 547 (2003).
[7] T.L. Hill and Y. Chen, Proc. Natl. Acad. Sci. USA **81**, 5772 (1984).
[8] G. Margolin, I. V. Gregoretti, H. V. Goodson and M. S. Alber, Phys. Rev. E **74**, 041920 (2006).
[9] H. Flyvbjerg, T. E. Holy and S. Leibler, Phys. Rev. Lett. **73**, 2372 (1994).
[10] C. Zong, T. Lu, T. Shen and P. G. Wolynes, Phys. Biol. **3**, 83 (2006).
[11] T. Antal, P. L. Krapivski and S. Redner, J. Stat. Mech. **May**, L05004 (2007).
[12] T. Antal, P. L. Krapivski, S. Redner, M. Mailman and B. Chakraborty, Phys. Rev. E **76**, 041907 (2007).

[13] P. Hinow, V. Rezania and J. A. Tuszyński, Phys. Rev. E **80**, 031904 (2009).
[14] P. Ranjith, D. Lacoste, K. Mallick and J. F. Joanny, Biophys J. **96**(6), 2146 (2009).
[15] I. M. Jánosi, D. Chrétien and H. Flyvbjerg, Biophys. J. **83**, 1317 (2002).
[16] M. I. Molodtsov, E. A. Ermakova, E. E. Shnol, E. L. Grishchuk, J. R. McIntosh and F. I. Ataullakhanov, Biophys. J. **88**, 3167 (2005).
[17] V. VanBuren, L. Cassimeris and D. J. Odde, Biophys. J. **89**, 2911 (2005).
[18] V. Hunyadi and I. M. Jánosi, Biophys. J. **92**, 3092 (2007).
[19] Y. Chen and T. L. Hill, Proc. Natl. Acad. Sci. USA **82**, 1131 (1985).
[20] P. M. Bayley, M. J. Schilstra and S. R. Martin, J. Cell Sci. **95**, 33 (1990).
[21] S. R. Martin, M. J. Schilstra and P. M. Bayley, Biophys. J. **65**, 578 (1993).
[22] B. M. Piette, J. Liu, K. Peeters, A. Smertenko, T. Hawkins, M. Deeks, R. Quinlan, W. J. Zakrzewski and P. J. Hussey, PLoS One **4**, e6378 (2009).
[23] P. T. Tran, P. Joshi and E. D. Salmon, J. Struct. Biol. **118**, 107 (1997).
[24] J. Howard and A. A. Hyman, Nature **422**, 753 (2003).
[25] H. T. Schek III, M. K. Gardner, J. Cheng, D. J. Odde and A. J. Hunt, Curr. Biol. **17**, 1445 (2007).
[26] E. B. Stukalin and A. B. Kolomeisky, J. Chem. Phys. **121**, 1097 (2004).
[27] J. Son, G. Orkoulas and A. B. Kolomeisky, J. Chem. Phys. **123**, 124902 (2005).
[28] L. Brun, B. Rupp, J, J. Ward and F. Nédélec F., Proc. Natl. Acad. Sci. USA. **106**, 21173 (2009).
[29] E. Nogales, K. H. Downing, L. A. Amos and J. Löwe, Nat. Struct. Biol. **5**, 451 (1998).
[30] D. K. Fygenson, E. Braun and A. Libchaber, Phys. Rev. E **50**, 1579 (1994).
[31] S. Pedigo and R. C. Williams Jr., Biophys. J. **83**, 1809 (2002).
[32] I. V. Gregoretti, G. Margolin, M. S. Alber and H. V. Goodson, J. Cell Sci. **119**, 4781 (2006).
[33] L.D. Landau and E.M. Lifshitz, *Statistical physics* Pergamon, London, 1980.
[34] D. Sept and J. A. Tuszyński, J. Biol. Phys. **26**, 5 (2000).
[35] M. Laurent and N. Kellershohn, Trends Biochem. Sci. **24**, 418 (1999).
[36] E. Nogales and H. W. Wang, Curr. Opin. Struct. Biol. **16**, 221 (2006).
[37] J. Howard, *Mechanics of Motor Proteins and the Cytoskeleton.* Sinauer Assoc., 2001.